Journal of Molecular Catalysis A: Chemical 333 (2010) 11–19

Contents lists available at ScienceDirect

Journal of Molecular Catalysis A: Chemical

journal homepage: www.elsevier.com/locate/molcata

Editor's Choice paper

Low temperature activation of Pt/Ni supported MCM-41 catalysts for hydrogenation of benzene

N.H.H. Abu Bakar[a,b], M.M. Bettahar[a,*], M. Abu Bakar[b], S. Monteverdi[a], J. Ismail[b]

[a] UMR CNRS-UHP 7565, IJB, Faculté des Sciences, Université Henri Poincaré, Nancy 1, BP 239, 54506 Vandoeuvre Cedex, France
[b] School of Chemical Sciences, Universiti Sains Malaysia, 11800 Gelugor, Penang, Malaysia

ARTICLE INFO

Article history:
Received 11 May 2010
Received in revised form
28 September 2010
Accepted 3 October 2010
Available online 4 November 2010

Keywords:
Pt/Ni catalysts
MCM-41
Aromatic hydrogenation
Anchoring effect
Kinetic investigations

ABSTRACT

A series of Pt/Ni supported MCM-41 catalysts prepared via classical methods have been investigated. The promotional effect of low activation temperature is shown in comparison to higher temperatures. Surface properties of the catalysts activated at low temperatures were studied using H_2-temperature programmed reduction (H_2-TPR), H_2-chemisorption and H_2-temperature programmed desorption (H_2-TPD) methods while the morphology and size distribution of the particles were obtained using transmission electron microscopy (TEM) analysis. Surface studies showed the promoting effect of Pt on the reduction of Ni species on the support. Total reduction only occurred for the Pt_{100} and $Pt_{90}Ni_{10}$ catalysts. Interestingly, it was found that the active phase of the monometallic catalysts were composed of spherical metal particles in the nanosize range, while the bimetallic catalysts showed a combination of spherical and large cubic particles. Tests on the gas phase hydrogenation of benzene show that $Pt_{50}Ni_{50}$ and $Pt_{90}Ni_{10}$ exhibit high activity when compared to Pt_{100}, though both these catalysts contain lower atomic percentages of Pt. This can be attributed to the anchoring effect of non-reduced Ni^{2+} ions that result in well dispersed Pt particles. Kinetic studies were conducted to understand the surface chemical process of the bimetallic catalysts.

1. Introduction

Aromatic compounds are known to be life threatening as they cause damages to the central nervous system and are carcinogenic. It is found in sources such as fuels and printing offices. Hence strict regulations have been enforced to ensure that only low concentrations of these substances are released into the environment. Oxidation and hydrogenation reactions have been employed as a means to reduce the amount of aromatic compounds [1,2].

The hydrogenation of aromatic compounds, have been investigated extensively over various catalysts such as Ni [3–6] and Pd [7]. In these studies, reduction techniques using hydrazine, sodium borohydride ($NaBH_4$) and H_2 gas have been employed. Even so, current trends have changed towards bimetallic catalysts such as Ni/Ag [2] and Ni/Zr [8]. This may be due to the synergistic effects, which may promote reactivity. In the case of Pt/Ni based systems, work have mainly been focused for reactions such as the oxidative steam reforming of methane [9,10], oxygen reduction reactions (ORR) [11,12], hydroisomerisation of n-heptane [13] as well as the hydrogenation of α,β-unsaturated aldehydes [14] and chloronitrobenzene [15]. In most cases the addition of Pt to Ni has shown an increase in the catalytic reactivity, regardless of the reaction employed. Generally, researches have described this enhanced activity as due to the formation of alloys which is known to effectively shorten the Pt–Pt neighboring distance which is favorable for oxygen adsorption in ORR [12], promote surface segregation of Pt [10] and cause an improved resistance to CO poisoning during methanol oxidation reaction [16].

For Pt/Ni supported catalysts, the studies that have given attention to the hydrogenation of benzene, examined in detail the sulfur tolerance of Pt/Ni supported on H-Mordenite (H-MOR) [17], as well as low temperature hydrogenation reactions of this bimetallic phase supported on γ-Al_2O_3 using flow and batch reactors [18]. Though in these works the Pt/Ni catalysts showed lower or slightly higher activity when compared to the monometallic Pt catalyst, we believe that the key to obtaining enhanced reactivity lies in controlling the properties of a catalyst which is influenced by varying factors such as the Pt/Ni ratio, the preparation techniques and their reduction conditions as we have shown for catalysts prepared via non-classical methods [19–21]. Other researchers have also shown similar findings, however for catalysts prepared via classical methods [22]. In the work conducted by Lonergan et al. [22] they found that co-impregnated Pt/Ni supported Al_2O_3 catalysts demonstrated an enhanced activity when compared to step-impregnated catalysts. Generally this was also observed in our previous works.

* Corresponding author. Tel.: +33 83 68 49 48; fax: +33 83 68 49 55.
E-mail address: mohammed.bettahar@lcah.uhp-nancy.fr (M.M. Bettahar).

1381-1169/$ – see front matter © 2010 Elsevier B.V. All rights reserved.
doi:10.1016/j.molcata.2010.10.007

Mesoporous molecular sieve MCM-41 has attracted widespread attention since its discovery in the early 1990s. Since then, this material has been established in many fields particularly in catalysis due to the large surface area it exhibits which promotes the formation of small dispersed particles. Work carried out by our research group indicates that a significant increase in the hydrogenation of benzene is observed when Ni is supported on MCM-41 in contrast to AlMCM-41 [3]. This is due to the higher extent of reduced Ni available on MCM-41 compared to AlMCM-41 which can be correlated to the strength of interaction. In contrast, other works in this lab showed that similar reactivity can be obtained when higher reduction temperatures are employed. However, the stability of the Ni–MCM-41 catalyst was drastically reduced [23]. These works show that the properties of metal supported MCM-41 based catalysts are largely influenced by the reduction conditions.

As the use of solely Pt as an active phase for hydrogenation reactions in catalysts is costly but well known to result in a high catalytic reactivity, studies to find potential alternatives is required. Based on the previous works in our lab [3], Ni supported MCM-41 based catalysts may hold promise as a low temperature activated catalyst when compared to catalysts supported on AlMCM-41. To enhance its catalytic reactivity and as an option to Pt supported catalysts, we describe a thorough study on the synthesis of Pt/Ni–MCM-41 catalysts. The catalysts were prepared via classical methods for the hydrogenation of aromatic compounds using benzene as a model feedstock. Various Pt/Ni ratios are investigated to determine the ratio of Pt/Ni in which optimum activity is obtained. Surface and structural properties including morphology of the catalysts are studied to understand how the metal phase influences reactivity. Kinetic studies are conducted to investigate the mechanism of reaction.

2. Materials and methods

2.1. Materials

The support, aluminosilicate, mesostructured hexagonal framework, MCM-41 was obtained from Aldrich while hexachloroplatinic acid ($H_2PtCl_6{\cdot}6H_2O$) was purchased from Sigma and nickel(II) sulphate ($NiSO_4{\cdot}6H_2O$) from R&M Chemicals.

2.2. Preparation of catalysts

Catalysts were prepared via co-impregnation techniques. Typically, as much as 5.0 g of MCM-41 was weighed and precipitated in 50 ml of distilled water. The precipitate was subjected to a flow of argon which was bubbled through the sample. Here, argon gas was employed to achieve an inert atmosphere as well as to act as a homogenizer for the sample. Subsequently, a previously determined amount of Ni stock solution was added followed by the Pt stock solution. The mixture was homogenized for another 15 min before evaporating the aqueous phase in an atmosphere of N_2 at 90–100 °C, until it was completely dried. Following this, it was calcined in air to oxidize the metal ions and remove impurities. The sample was placed in a U shaped reactor and heated to 373 K at a heating rate of 5 K min^{-1} in a flow of 300 ml min^{-1} air. Treatment was allowed to continue at this temperature for 1 h before increasing the temperature to 773 K at a heating rate of 30 K min^{-1}. Samples were calcined for duration of 4 h before activation and subsequent catalytic analysis and characterization.

2.3. Characterization techniques

Reducibility of the calcined catalysts was investigated using H_2-TPR analysis. 50 mg of a sample was weighed and placed in a reactor. A gas flow of 90 ml min^{-1} diluted hydrogen was than passed through the reactor while heating at a rate of 5 K min^{-1} to 1123 K. The resulting effluent gas was analyzed every 2 min using an Agilent G2890A microchromatograph operated at 333 K.

Surface characteristics were also studied via H_2-chemisorption and H_2-TPD. The treated samples were previously activated by heating the catalysts at a constant rate of 10 K min^{-1} to 373 K in a flow of 100 ml min^{-1} pure hydrogen. The temperature was held at 373 K for another 3 h and then the hydrogen was switched to argon with similar flow rate. The system was purged with argon for approximately 45 min and then cooled to room temperature. Subsequently, the sample was adsorbed with H_2 for H_2-chemisorption studies. Upon saturation, the gas flow was switched to argon and the system was purged until no H_2 was detected. H_2-TPD analysis was then conducted by heating the catalyst at a rate of 5 K min^{-1} to 1123 K in a flow of 100 ml min^{-1} argon. Similar temperature program and gas chromatograph as for the TPR studies were employed for both the H_2-chemisorption and H_2-TPD studies.

The degree of oxidation was determined by chemisorption of oxygen at high temperature [24]. It was investigated using 50 mg of a catalyst and activating the catalyst under similar conditions as for the H_2-chemisorption and H_2-TPD analyses. After activating for 3 h at 373 K, the gas flow was switched to 100 ml min^{-1} of argon. The sample was purged for duration of 1 h. The temperature was then further increased to 673 K at a ramp of 10 K min^{-1} in argon. Upon reaching 673 K, the gas flow was switched to diluted oxygen (100 ppm O_2) with a flow rate of 100 ml min^{-1}. The chemisorption of O_2 was analyzed every 2 min using a similar gas microchromatograph as for the TPR. The reduction reaction is assumed to occur as in the following reactions.

$$Pt^{\circ} + \frac{1}{2}O_2 \rightarrow PtO$$

$$Ni^{\circ} + \frac{1}{2}O_2 \rightarrow NiO$$

Degree of reduction was calculated by dividing the total mol of oxygen involved in the reaction with the total mol of metal content.

Transmission electron micrographs were obtained by redispersing the catalysts in ethanol. A drop of the mixture was then placed onto carbon coated copper grids and analyzed using a Philip CM 12 TEM operating at 80 kV and a Philips CM 20 TEM operating at 20 kV equipped with EDX. In contrast, X-ray diffraction (XRD) analyses were performed using the catalysts as obtained. A SIEMENS D5000 X-ray diffractometer equipped with a monochromatic Cu Kα radiation filter was employed to scan the samples in the 2θ range of 0–100°.

2.4. Catalytic activity

Gas phase hydrogenation of benzene was conducted using 50 mg of the previously calcined sample. Samples were placed in a U shaped reactor and activated in a flow of 100 ml min^{-1} pure hydrogen. In this case, samples were heated at a heating rate of 10 K min^{-1} to 373 K and then held at the same temperature for duration of 3 h. Upon activation, the catalyst was cooled to room temperature before exposing the sample to a reaction flow of He/H_2/benzene (150/40/10 ml min^{-1}). Catalytic activity was investigated as a function of temperature. The resulting gas was detected using a 5730A Hewlett-Packard gas chromatography (GC) equipped with a flame ionization detector.

2.5. Kinetic studies

The energy of activation measurement was performed using a similar set-up as the hydrogenation of benzene. However, 25 mg of the catalyst was placed into a reactor and heated to 373 K at a

Table 1
Maximum conversions and temperatures at maximum conversion of the $Pt_{50}Ni_{50}$ catalyst activated at various conditions.

Conditions				Maximum conversion (%)	Temp. at maximum conversion (K)
Temp. (K)	Activation time (h)	Flow rate (ml min^{-1})	Ramp (K min^{-1})		
373	3	100	10	42.3	458
473	3	100	10	24.7	474
373	2	100	10	35.3	489
373	4	100	10	33.6	439
373	3	200	10	37.2	467
373	3	100	5	33.4	448

constant rate of 10 K min^{-1} in 50 ml min^{-1} of pure hydrogen for duration of 3 h. Subsequently, the catalyst was cooled to 323 K and the hydrogenation of benzene was conducted in the temperature range of 323–498 K. A reaction flow of benzene/hydrogen/helium (9/50/141 ml min^{-1}) was employed.

The reaction orders of benzene and hydrogen were determined in separate experiments. Typically, 25 mg of catalyst was activated in similar conditions as for the determination of the energy of activation. Subsequently, to obtain the reaction order of benzene, the catalyst was cooled to 358 K and reactions were carried out in a series of reaction mixtures containing various flow rates of benzene (5–15 ml min^{-1}) while maintaining the hydrogen flow rate at 50 ml min^{-1}. Helium was used to mark up the total flow rate to 200 ml min^{-1}. After each reaction, catalyst was cleaned in a flow of hydrogen while heating at 373 K before cooling to 358 K and continuing with the following reaction mixture. In the same way, the reaction order of hydrogen was obtained, however the flow rate of hydrogen was varied between 25 and 40 ml min^{-1} while maintaining the flow rate of benzene at 10 ml min^{-1} and adding helium to obtain a total flow rate of 200 ml min^{-1}.

Temperature programmed surface reaction (TPSR) studies were carried out on 25 mg of a used sample. The sample was activated in a flow of 50 ml min^{-1} pure hydrogen from room temperature to 373 K at a heating rate of 10 K min^{-1} for 3 h. The hydrogenation of benzene was then carried out at 323 K in a reaction flow of 5/50/145 ml min^{-1} C_6H_6/H_2/He. Following this, the sample was cooled to room temperature while helium was passed through the reactor for duration of 1 h. The amount of reversibly adsorbed benzene was monitored via a GC. To investigate the amount of irreversibly adsorbed benzene, temperatures were then increased at a rate of 2 K min^{-1} and in a flow of 2/48 ml min^{-1} H_2/He from room temperature to 673 K.

3. Results and discussion

3.1. Effect of activation conditions

The $Pt_{50}Ni_{50}$ catalyst was employed to determine the optimum activation conditions for the series of catalysts investigated, as similar weight compositions of the Pt and Ni was incorporated in this catalyst. This enabled us to obtain a balance between the conditions required to activate Pt (usually low temperature activation) and Ni (activation at higher temperature).

The activity of the catalyst was compared at different activation temperatures, time and temperature ramps. Maximum conversion and the temperature at which it is achieved are tabulated in Table 1. As can be seen, the catalyst activated at 373 K for duration of 3 h (100 ml min^{-1}, 10 K min^{-1}) showed the highest conversion of approximately 42.3% at 458 K. Catalysts activated at 473 K showed only two thirds the conversion of that activated at 373 K. The drastic decrease in activity as temperature is increased can be attributed to the formation of aggregates which is well known to occur at higher activation temperatures. Oxygen chemisorption confirms this (see Section 3.2). Also considering that high activation temperatures resulted in lower activity, all catalysts in the following discussions were treated at 373 K for duration of 3 h (100 ml min^{-1}, 10 K min^{-1}) when activation was required.

3.2. O_2-chemisorption

O_2-chemisorption studies were carried out to determine the degree of reduction of the metal phase for the $Pt_{50}Ni_{50}$ catalysts activated at 373 and 473 K for duration of 3 h (100 ml min^{-1}, 10 K min^{-1}) as well as for the catalysts with different Pt/Ni ratios after activation at 373 K in pure hydrogen. The degree of reduction obtained for catalysts with different Pt/Ni ratios are shown in Table 2.

The $Pt_{50}Ni_{50}$ catalyst activated at 373 and 473 K adsorbed 7.26×10^{-3} and 9.42×10^{-3} mol g_{met}^{-1} O_2 respectively. This corresponds to 65.7% and 85.0% of the metallic phase existing in a reduced state. Indirectly, this indicates the formation of aggregates when higher activation temperatures are carried out. Aggregates interact less with the support and are therefore more prone to oxygen attack. This confirms the above conclusion that aggregation of the metal particles upon activation gives rise to a lower activity for the catalysts activated at 473 K.

It was found that the Ni_{100} catalyst exhibited the lowest degree of reduction. Only 1.17×10^{-3} mol g_{met}^{-1} of O_2 was adsorbed attributing to 6.8% of the Ni phase existing as Ni$^{\circ}$ after activation. The $Pt_{10}Ni_{90}$ catalyst on the other hand showed an O_2 adsorption of 1.88×10^{-3} mol g_{met}^{-1}. This demonstrates a degree of reduction of 12.0%. The low degree of reduction in both the Ni_{100} and $Pt_{10}Ni_{90}$ catalysts can be ascribed as due to both the low calcination and activation temperatures. The calcination temperature employed in this work prevents total decomposition of nickel sulfate to nickel oxides. Based on previous work [25], it has been shown that nickel

Table 2
H_2-chemisorption, dispersion, average particle size and degree of metal reduction of the Pt/Ni catalysts supported MCM-41.

Catalyst	Total metal content (wt%)	Metal loading (%)		H_2-adsorption ($\times 10^{-3}$ mol g_{met}^{-1})	Dispersion[a] (%)	Particle size[a] (nm)	Degree of metal reduction (%)
		Pt	Ni				
Ni_{100}	0.80	–	0.80	0.13	21.8	4.6	6.8
$Pt_{10}Ni_{90}$	0.90	0.10	0.80	0.07	6.8	14.7	12.0
$Pt_{50}Ni_{50}$	0.90	0.45	0.45	1.43	42.3	2.7	65.7
$Pt_{90}Ni_{10}$	0.70	0.60	0.10	1.96	38.2	2.9	105.0
Pt_{100}	1.10	1.10	–	1.02	19.9	5.6	103.0

[a] Obtained from H_2-chemisorption studies after taking into account the degree of reduction of the catalyst.

sulfate usually decomposes at calcination temperatures of approximately 1003 K and above. This limits the availability of NiO for subsequent reduction with H_2. In addition, the low activation temperature may contribute to insufficient energy for H_2 to reduce the nickel oxides to Ni° nanoparticles.

In contrast the Pt_{100} and $Pt_{90}Ni_{10}$ catalysts adsorbed 5.36×10^{-3} and 7.00×10^{-3} mol g_{met}^{-1} respectively. The calculated degree of reduction gives the respective values of 105 and 103% of the metal phase existing in the reduced state. In both cases, we consider that 100% of the metal phase is reduced after activation. Medium degree of reduction is obtained with the $Pt_{50}Ni_{50}$ catalyst.

3.3. Surface characteristics

3.3.1. H_2-TPR

H_2-TPR profiles of the catalysts after calcinations at 773 K are illustrated in Fig. 1. The profile of Ni_{100} supported on MCM-41 exhibits a strong sharp peak positioned at approximately 800 K. This peak can be attributed to the occurrence of NiO [26], nickel silicate [3] or nickel sulfate [27] in the catalysts which are in strong interaction with the support. In contrast, the Pt_{100} supported MCM-41 catalyst can be characterized by a small peak positioned at 374 K. Decomposition of PtO_2 can occur at temperatures ranging between 553 and 823 K [28,29]. In this work, calcination was conducted at 773 K hence decomposition of PtO_2 to form Pt and O_2 may have occurred as previously reported [30]. This may have caused reduction of a majority of the PtO_2 hence resulting in the small peak observed. Previous works have shown that the consumption of hydrogen in this temperature region is explained as due to the reduction of PtO or PtO_2 [31]. The position of this peak varies depending on the support employed as well as the addition of a metal [31,32]. Further observation of the profile also reveals the presence of another two different metal particle sizes or sites in the Pt_{100} catalysts. Interestingly, these two sites which appear at about 693 and 894 K exhibit the production of hydrogen. This phenomenon can be attributed to the desorption of hydrogen incorporated at lower temperatures during H_2-TPR analysis. Hydrogen dissociates at the surface of the Pt particles and then migrates to the MCM-41 support as spillover hydrogen. As the temperature is increased, enough energy is obtained to allow desorption of the hydrogen from the support.

The surface properties of the bimetallic catalysts after calcination are dependent on the metal ratios. Typically, they show

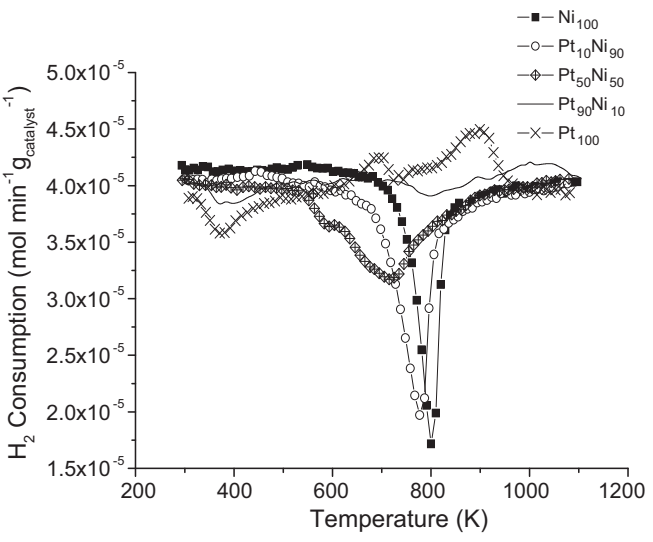

Fig. 1. H_2-TPR profiles of Pt/Ni supported MCM-41 catalysts prepared at various Pt/Ni ratios.

intermediate characteristics of the pure metal supported MCM-41 catalysts. It can be observed that the $Pt_{10}Ni_{90}$ catalyst demonstrates a peak similar to that of the Ni_{100} catalyst. This peak may also arise due to the existence of nickel oxides, nickel silicates or residual nickel sulfate with MCM. However, the peak is slightly shifted to a lower temperature of 777 K. The slight shift may be attributed to the hydrogen spillover effect. The spillover species which originates from the Pt particles migrates to the Ni species via the support facilitating the reduction of the nickel species at lower temperatures. Segregates of Pt and Ni species are expected to exist on the support ensuring the transport of hydrogen [33]. A comparable trend is also seen for the $Pt_{50}Ni_{50}$ catalyst. Here, a main peak and a shoulder are positioned at 718 and 593 K respectively. The $Pt_{90}Ni_{10}$ catalyst on the other hand exhibits characteristics similar to the Pt_{100} catalyst. A slight consumption peak arises at approximately 381 K. In addition, hydrogen spillover occurs at higher temperatures, tough to a lesser extent when compared to the Pt_{100} catalyst.

3.3.2. H_2-chemisorption studies

H_2-chemisorption studies were carried out to obtain information on the dispersion of the metal phase. Values are tabulated in Table 2. Corrections have been made taking into account the degree of reduction of the catalysts.

As can be seen, catalysts with low quantities of Pt (Ni_{100} and $Pt_{10}Ni_{90}$) exhibit low hydrogen adsorption at room temperature. Upon taking into consideration the degree of reduction, it can be seen that the Ni_{100} catalyst exhibits a dispersion of 21.8% giving a large metal surface area of 145.6 $m^2\ g^{-1}$. Due to low degree of reduction, the matrix allowed the stabilization of very small Ni° particles. Low activation temperature prevented their aggregation. The $Pt_{10}Ni_{90}$ on the other hand gives rise to a lower dispersion. Higher degree of reduction in $Pt_{10}Ni_{90}$ led to excess of Ni° atoms formed which are more easily agglomerated than in Ni_{100}.

In contrast, the $Pt_{50}Ni_{50}$ catalyst as well as catalysts with high amounts of Pt content ($Pt_{90}Ni_{10}$ and Pt_{100}) demonstrates a H_2 adsorption of more than 10 times that exhibited by the Ni_{100} catalyst. Dispersion of these catalysts range between 19.0 and 43.0%.

Interestingly it is observed that both the $Pt_{50}Ni_{50}$ and $Pt_{90}Ni_{10}$ catalysts exhibit enhanced hydrogen adsorption characteristics when compared to the Pt_{100} catalyst. This may be attributed to the smaller size of the metal particles which can give rise to a larger surface area of the metal phase available for reaction. This promotes hydrogen adsorption. The small sizes can be explained as due to the anchoring effect of the Ni^{2+} ions that aides the formation of well dispersed Pt particles. Less reducible metal acts as anchors for more reducible metals [34]. According to Yermakov et al., Pt particles can be stabilized by Re ions, which act as anchoring sites on SiO_2 [35]. Other researches have also explained this phenomenon in detail [34,36].

3.3.3. H_2-TPD

The H_2-TPD curves of the catalysts are presented in Fig. 2. The profile of the Ni_{100} catalyst shows a very low desorption of hydrogen which reaches a maximum at 494 and 660 K. Both peaks are broad, indicating the availability of a wide range of Ni particle size upon activation in pure hydrogen or the existence of different Ni species with various adsorption strengths. The low quantities of hydrogen desorbed can be attributed to the small number of Ni°. The Pt_{100} on the other hand reveals very large hydrogen desorption in the temperature range of approximately 400–1073 K. Here, optimum desorption occurs at 675 and 800 K. Shoulders which signify the presence of other active sites are also seen at 474 K and after 920 K. Generally, it has been proposed that the shoulder at 474 K can be attributed to hydrogen chemisorbed on the Pt surface [37] while the peaks at higher temperatures correspond to the hydrogen species on the support far from the Pt, namely hydrogen

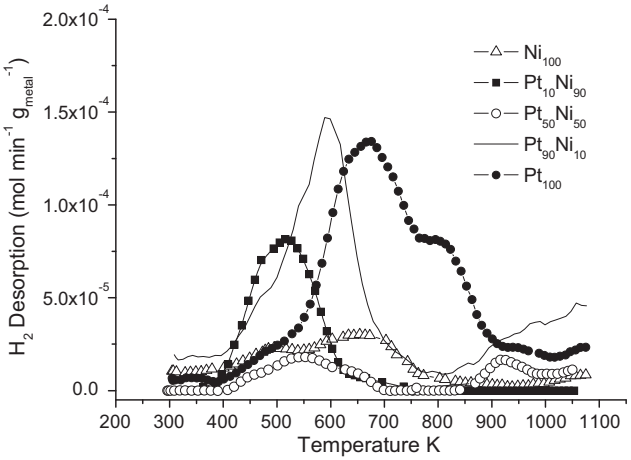

Fig. 2. H_2-TPD profiles of Pt/Ni supported MCM-41 catalysts prepared at various Pt/Ni ratios.

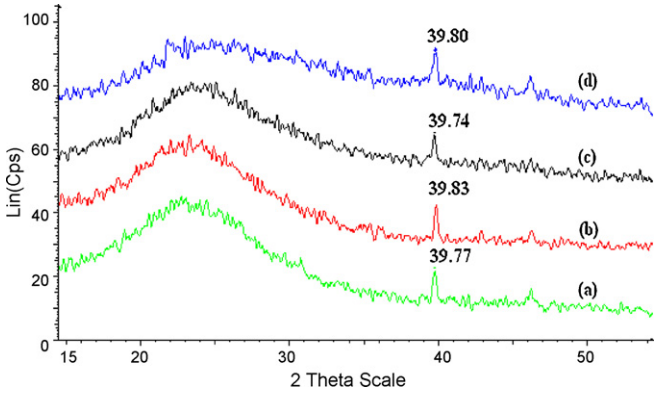

Fig. 3. XRD spectra of (a) Pt_{100} and (b) $Pt_{90}Ni_{10}$ before as well as (c) Pt_{100} and (d) $Pt_{90}Ni_{10}$ after benzene hydrogenation reactions.

spillover. This correlates well with the H_2-TPR curves. Comparison of the amount of hydrogen desorbed from the Pt_{100} catalyst with that of the Ni_{100} demonstrates that a larger quantity is desorbed from the Pt_{100} catalyst. This occurrence can be attributed to a greater number of Pt° atoms and a better dispersion of the metal particles in the Pt_{100} catalyst which increases the amount of hydrogen atoms incorporated on the metal or the support surface as spiltover species.

The profiles of the Pt/Ni supported MCM catalysts are also depicted in Fig. 2. The $Pt_{10}Ni_{90}$ catalyst exhibits a peak at 516 K. In contrast, the $Pt_{50}Ni_{50}$ and $Pt_{90}Ni_{10}$ catalysts give rise to two peaks positioned as 542 and 918 K as well as 590 and starting at 835 K correspondingly. The peaks positioned in the temperature range of 510–590 K in all three bimetallic catalysts are consistent with H_2 moderately attached to the metal surface. It can be seen that the temperature at which maximum desorption occurs in these catalysts, shifts to lower temperatures with increasing Ni content. This demonstrates the synergistic effect between Pt/Ni. Furthermore, except for the $Pt_{50}Ni_{50}$ catalyst, it is generally seen that the amount of desorbed hydrogen decreases with increasing Ni content. This demonstrates the decrease of the number of Ni° atoms with increasing Ni content, which causes a decrease in the metallic surface area available for adsorption to occur. The exceptional behavior of the $Pt_{50}Ni_{50}$ catalyst is not fully understood.

3.4. Structural properties

XRD analysis was conducted to investigate the nature in which the metallic phase of Pt/Ni exists. Spectra of the Pt_{100} and $Pt_{90}Ni_{10}$ before and after hydrogenation reaction are exhibited in Fig. 3. The spectra demonstrate a broad peak positioned at the 2θ value of approximately 23°. This peak is assigned to the MCM-41 support. The total metal content in the catalysts are low. However, further inspections of the spectra reveal that metallic peaks are available. This may be due to particle–particle interactions when metal particles exist in close proximity to each other or due to the availability of large or aggregated metal particles. As can be seen, the Pt_{100} and $Pt_{90}Ni_{10}$ catalysts before hydrogenation reactions (obtained after calcinations in air) give rise to peaks positioned at ~39.77° and ~39.83° respectively. These diffraction peaks can be indexed to the (1 1 1) phase of the face cubic centered (fcc) structure of metallic Pt. No peaks indicating the presence of PtO_2 or Pt_3O_4 are available [38]. This can be explained as due to the decomposition of the majority of the platinum oxides during calcinations as previously mentioned. The low content of platinum oxides as shown by H_2-TPR studies may not be observable in the XRD diffractograms. Further inspections show that a slight shift towards higher 2θ values is seen in the spectrum of $Pt_{90}Ni_{10}$ when compared to the pure Pt catalyst. This can be explained as due to the occurrence of lattice distortions of the fcc structure of Pt. These lattice distortions have been related to the formation of alloys [39,40] as well as a variation in particle structure. Comparison of the $Pt_{90}Ni_{10}$ and Pt_{100} catalysts supported on MCM-41 after hydrogenation reaction also show similar trends to that of the catalysts obtained before hydrogenation reaction.

3.5. Morphological studies

The morphology of the active phase of the Pt/Ni supported MCM-41 catalysts before and after catalytic reactions was investigated via TEM. Images of the catalysts before catalytic reactions were obtained after impregnation of the metal salts as well as after subsequent calcination in air. TEM investigations show that the metal particles are formed on the outer surface of the MCM-41 support. Formation of metal particles in the MCM-41 pores, if any, is unknown. Typically, it is observed that fine flat like spherical particles are obtained upon impregnation of the metal salts (figure not shown). These grain-like particles grow upon heat treatment during calcination forming larger particles. Interestingly it is found that a variety of particle shapes are observed in the bimetallic catalysts while only spherical particles exist in both the Pt_{100} and Ni_{100} catalysts. Similar particle morphologies are also observed after catalytic reactions. The occurrences of the particles were infrequent. This may be due to the low quantity of metal incorporated onto the support.

The shape distribution and average particle size of the metal particles in the catalysts after calcinations and after hydrogenation reactions are tabulated in Table 3(a) and (b) respectively.

Table 3
Average particle sizes and distribution of particle shapes of the metallic phase in the Pt/Ni catalysts (a) before and (b) after hydrogenation reactions.

Catalysts	Average particle size (nm)		% Cubes	% Spherical
	Spherical	Cubes		
(a)				
Ni_{100}	1.6 ± 0.9	–	–	100
$Pt_{10}Ni_{90}$	3.7 ± 1.3	6.7 ± 2.2	7.0	93.0
$Pt_{50}Ni_{50}$	10.4 ± 13.2	51.9 ± 20.6	15.9	84.1
$Pt_{90}Ni_{10}$	1.9 ± 0.4	17.1 ± 5.4	19.6	80.4
Pt_{100}	1.6 ± 0.6	–	–	100
(b)				
Ni_{100}	2.3 ± 0.7	–	–	100
$Pt_{10}Ni_{90}$	3.9 ± 1.8	13.6 ± 4.4	13.2	86.6
$Pt_{50}Ni_{50}$	1.8 ± 1.6	19.4 ± 10.5	10.0	90.0
$Pt_{90}Ni_{10}$	1.6 ± 0.3	16.2 ± 10.3	7.4	92.6
Pt_{100}	1.4 ± 1.3	–	–	100

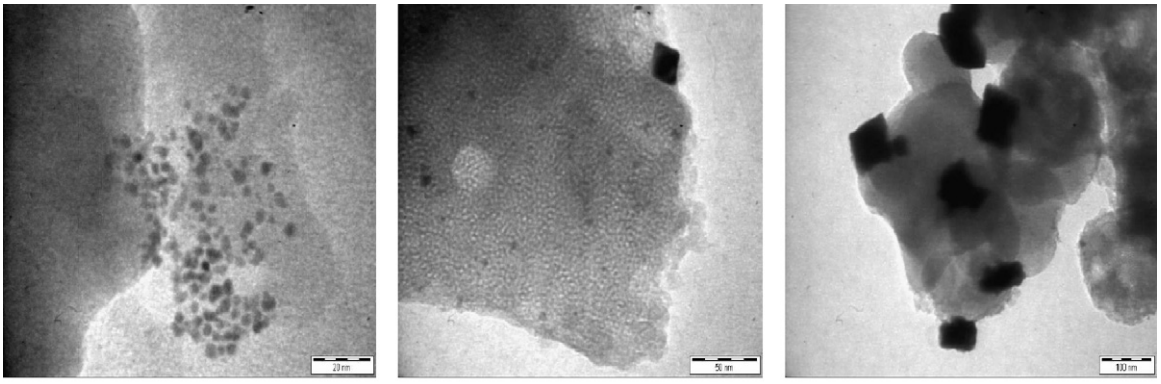

Fig. 4. Typical TEM images of the various morphologies (a) spherical (b) mixtures of spherical and rectangular and (c) rectangular nanoparticles in the catalysts.

As can be seen, both the Pt_{100} and Ni_{100} calcined catalysts are composed of spherical nanoparticles with average particle sizes of 1.6 ± 0.6 and 1.6 ± 0.9 nm correspondingly. In the Ni_{100} catalyst, particles which are well distributed on the MCM-41 support are small in size. This is unusual considering that Ni species such as its oxide, is prone to aggregation due to its magnetic properties. Even so, this occurrence may be explained as due to the strong interaction between the metal species and the support. Previous works have shown similar findings [3]. The low Ni content and high surface area of the support may have resulted in a large amount of the Ni species attached directly to the support. Our findings correlate well with the H_2-TPR and H_2-TPD profiles discussed above.

The calcined bimetallic Pt/Ni supported MCM-41 catalysts give rise to nanoparticles with different morphologies. Typical TEM images of the different morphologies are exhibited in Fig. 4. In all the catalysts, mixtures of spherical and rectangular nanoparticles exist. The distribution of rectangular nanoparticles varies between 6 and 20%. Average particle sizes of the rectangular particles are 17.1 ± 5.5, 51.9 ± 20.6 and 6.7 ± 2.2 nm for the $Pt_{90}Ni_{10}$, $Pt_{50}Ni_{50}$ and $Pt_{10}Ni_{90}$ catalysts respectively. Here, particle size increased from 10 to 50 wt% of Ni content and then decreased with further increase in Ni content. A similar trend was also observed for the spherical nanoparticles. However, the spherical particles are much smaller in size. Average particle size of the spherical nanoparticles for the $Pt_{90}Ni_{10}$, $Pt_{50}Ni_{50}$ and $Pt_{10}Ni_{90}$ catalysts are 1.9 ± 0.4, 10.4 ± 6.3 and 3.7 ± 1.3 nm correspondingly.

Upon activation and subsequent catalytic reactions, it is observed that the average particle sizes in both the Pt_{100} and Ni_{100} catalysts did not vary drastically when compared to those obtained before catalytic reactions. Average particle sizes of the metal phases are 1.4 ± 0.3 and 2.3 ± 0.7 nm respectively. For the Ni_{100} catalyst, this observation strengthens our belief that particles in this catalyst are strongly attached to the support, possibly via Ni^{2+} ions. This inhibits migration and subsequent aggregation of the metallic particles upon reduction or catalytic reaction. To demonstrate this, TEM equipped with EDX analysis was conducted on several areas of the support in the Ni_{100} catalyst where particles were not observed. In all the areas investigated, it was found that trace amounts of Ni were detected as shown in Fig. 5(a). This proves that very fine Ni species are available on the MCM-41 support, probably in the forms of ions, in accordance with the low degree of reduction as determined by chemisorption of oxygen (Table 2). When the Pt_{100} catalyst was analyzed in the same way, such findings were not obtained. In contrast, Pt was only detected by EDX when particles are observed as in Fig. 5(b). This suggests that Pt ions less interacted with the support. In comparison to the monometallic catalysts, the bimetallic catalysts exhibit severe changes in the average particle sizes, though similar distributions in the particle shapes are observed. In this case the average particle sizes of the rectangular and spherical particles decreased to 13.0–20.0 nm as well as 1.6–4.0 nm correspondingly, depending on the Pt/Ni ratio. This may be attributed to large agglomerated species formed during calcination which split to smaller particles under a hydrogen flow or reductive atmosphere. This would be particularly the case for $Pt_{50}Ni_{50}$.

It is interesting to note that only the bimetallic catalysts exhibit particles with various morphologies. This could explain the shift in the XRD spectra of the $Pt_{90}Ni_{10}$ catalyst relative to the Pt_{100}. To explain this observation we take into consideration the oxidizing role of the Ni^{2+} ions in the system. We propose that these ions either manipulate the decomposition kinetics of the PtO_2 by re-oxidizing the Pt atoms or seeds formed as temperatures are increased during calcination or adsorb onto certain phases of the Pt nanocrystals. Either way, this causes the growth of the Pt particles to occur along certain surfaces, leading to the morphologies observed. Similar behavior has been observed by other researches who studied the effect of Fe^{3+} ions [41] and Ag^{2+} ions [42] on the morphology of Pt nanoparticles.

3.6. Catalytic activity

The gas phase hydrogenation of benzene produced only cyclohexane, indicating that total hydrogenation occurred over the catalysts prepared. Profiles of the reaction rates as a function of temperature are illustrated in Fig. 6. Under the conditions employed Ni_{100} exhibited no activity at all. This is expected even though the average particle sizes of the Ni nanoparticles formed after calcination have an average diameter of 1.6 ± 0.9 nm. The inactivity of this catalyst can be attributed to the activation temperature and the strength of interaction between the metal and the support. The low activation temperature is insufficient to reduce the metal species which strongly interacts with the support hence affects the metallic area available for the reaction to occur. This observation correlates well with the O_2-chemisorption and H_2-TPR analysis. Similar findings have been reported by Lewandowska et al. [23].

The increase of Pt content in the catalysts leads to an increase in the reaction rates. $Pt_{10}Ni_{90}$ exhibited only a slight increase starting at approximately 350 K and reaching a maximum reaction rate of 0.77×10^{-3} mol min^{-1} g_{met}^{-1} at 416 K before declining. In contrast, drastic enhancements in the reaction rates are seen when the Pt content is further increased. The $Pt_{50}Ni_{50}$ and $Pt_{90}Ni_{10}$ catalysts were found to be active even at 298 K. Here, reaction rates increased reaching a maximum of 21.03×10^{-3} mol min^{-1} g_{met}^{-1} and 53.65×10^{-3} mol min^{-1} g_{met}^{-1} at 458 K and 452 K respectively. The reaction rates of the $Pt_{90}Ni_{10}$ catalyst was found to be higher than that of

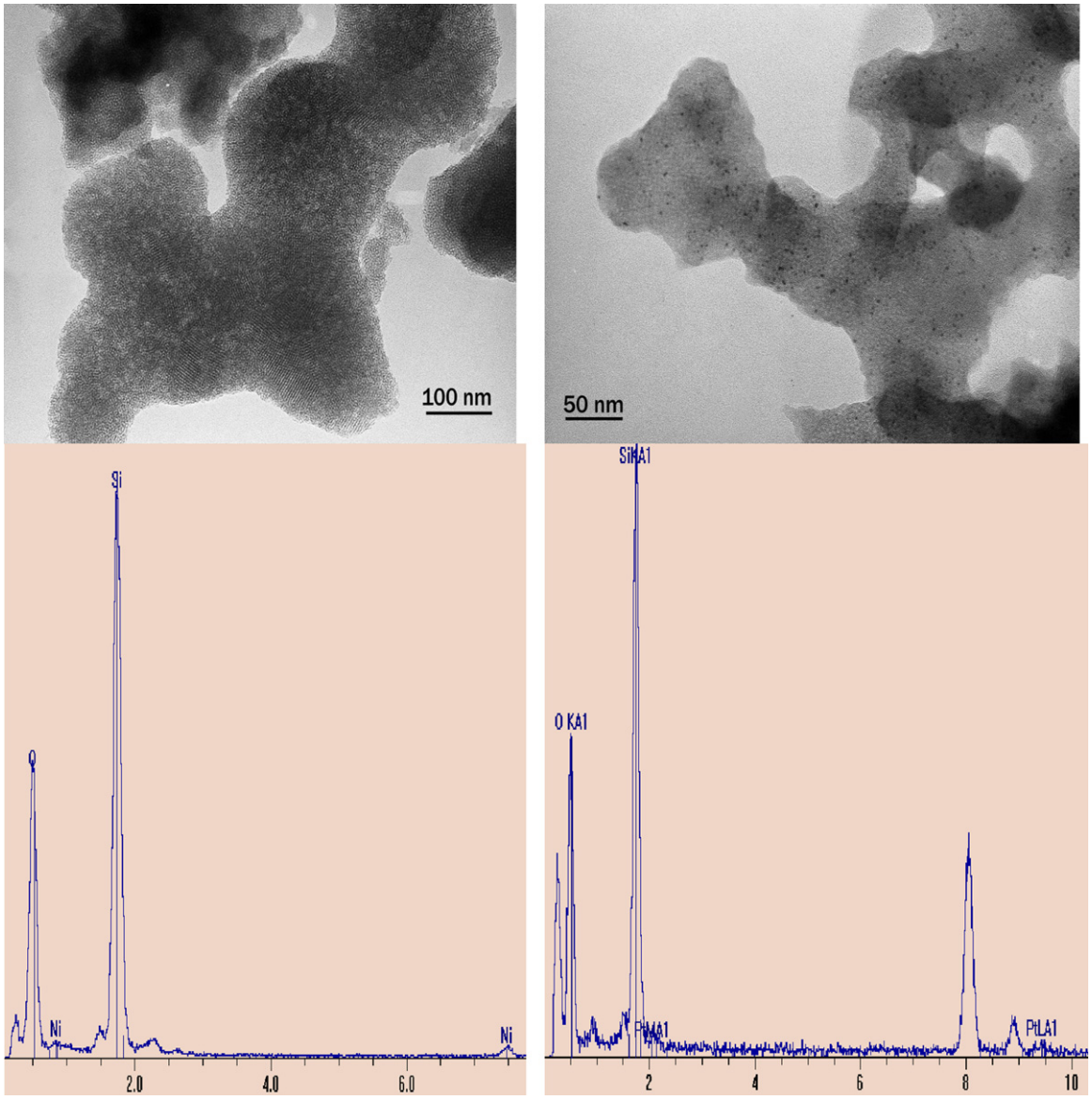

Fig. 5. TEM images of typical areas in the (a) Ni_{100} and (b) Pt_{100} catalysts as well as their corresponding EDX analysis.

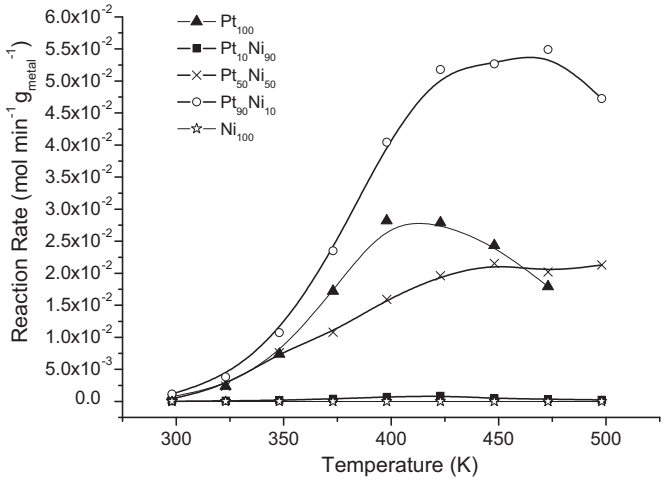

Fig. 6. Profiles of the reaction rate of hydrogenation of benzene to cyclohexane for various Pt/Ni catalysts supported on MCM-41 relative to the reaction temperature.

Pt_{100}, which demonstrated a maximum reaction rate of 27.08×10^{-3} mol min^{-1} g_{met}^{-1} at 412 K. It is also interesting to note that the $Pt_{50}Ni_{50}$ catalyst gave rise to reaction rates that were similar to that of Pt_{100} despite the fact that only 65.7% of the catalyst existed in a reduced state and that only half the Pt content is available. These enhanced reaction rates can be explained as due to the anchoring effect of the Ni^{2+} ions that aides the formation of well dispersed Pt particles as reported above.

The turnover frequency (TOF) values were calculated to gain an insight on the number of benzene molecules converted to cyclohexane on a catalytic site per second. This is tabulated in Table 4. Inactivity prevented the determination of this value for the Ni_{100} catalyst. However, the calculated TOF value for the $Pt_{10}Ni_{90}$ catalyst is 0.020 s^{-1}. Interestingly, the $Pt_{50}Ni_{50}$ and $Pt_{90}Ni_{10}$ catalysts show lower TOF values when compared to the Pt_{100} catalyst. In these cases, the TOF value of Pt_{100} is approximately 0.030 s^{-1} more than the $Pt_{50}Ni_{50}$ and $Pt_{90}Ni_{10}$, though an enhanced reactivity was seen for the latter catalysts. Based on these findings it is obvious that the Pt sites in the Pt_{100} catalysts are more reactive than those available in the bimetallic catalysts. However, the improved reactivity of the $Pt_{50}Ni_{50}$ and $Pt_{90}Ni_{10}$ catalysts may be ascribed as due

Table 4
Percentage of conversion, specific rates and TOF values of the Pt/Ni supported MCM-41 catalysts prepared with various Pt/Ni ratios.

Catalysts	Maximum conversion (%)	Max. specific rate ($\times 10^{-3}$ mol min^{-1} g_{met}^{-1})	Temp. at max. specific rate (K)	Specific rate at 350 K ($\times 10^{-3}$ mol min^{-1} g_{met}^{-1})	TOF (s^{-1}) at 350 K
Ni_{100}	–	–	–	–	–
$Pt_{10}Ni_{90}$	1.8	0.77	416	0.17	0.020
$Pt_{50}Ni_{50}$	42.3	21.03	458	7.62	0.089
$Pt_{90}Ni_{10}$	85.4	53.65	452	10.72	0.091
Pt_{100}	74.0	27.08	412	7.41	0.121

to the availability of a larger amount of reaction sites as shown by H_2-chemisorption studies.

3.7. Kinetic investigations

The apparent energy of activation (E_a) was obtained for the $Pt_{50}Ni_{50}$ catalyst. Conversions were ensured to be less than 10%, to limit deactivation of the catalysts during investigations. It is found that the E_a of the $Pt_{50}Ni_{50}$ catalysts is 24.4 kJ mol^{-1}. Comparison with previous works showed that this value is lower than that of both Pt and Ni monometallic supported catalysts which have been reported to be 50.3 kJ mol^{-1} [43] and 36.5–96.0 kJ mol^{-1} [22,44,45] correspondingly. In addition, this value is less than half of that reported by Lu et al. [18] who studied the synthesis of Pt/Ni supported γ-Al_2O_3 catalysts for the hydrogenation of benzene. In their work, an E_a value of approximately 56.8 kJ mol^{-1} was obtained. We acknowledge that the difference in the total metal content, the Pt/Ni ratio or nature of the support may have caused this variation in the activation energy. Metal dispersion of $Pt_{50}Ni_{50}$ supported on MCM-41 (42.3%) was much higher then that of 1.2Pt10Ni (percentage based on total metal content is $Pt_{11}Ni_{89}$) supported on γ-Al_2O_3 (7.5%). The smaller metal particles in $Pt_{50}Ni_{50}$ sharply increased the reactivity of surface atoms and hence dramatically decreased the energy of activation. Calculations using H_2 chemisorption measurements showed that the TOF of $Pt_{50}Ni_{50}$ is 22 times higher than that of the latter at similar reaction temperature.

The very low value of the apparent energy of activation may suggest the presence of diffusion limitations. However, formation of strongly chemisorbed species may also give rise to a chemical process step of very low energy level and hence may dramatically decrease the apparent energy of activation. Kinetics and TPSR experiments give some evidence in this sense.

Experimental reaction orders were calculated based on the empirical kinetic model,

$$r = kP_H^m P_{Bz}^n \quad (1)$$

where m and n are the partial orders of hydrogen and benzene correspondingly and k is the rate constant. Experimental results indicate that reaction orders of hydrogen and benzene is 1.6 and −0.5 respectively. These reaction orders are consistent with previous works which report values ranging from 1.0 to 2.0 and −1.7 to 0.30 correspondingly [3,46]. The negative order of benzene indicates that benzene is strongly adsorbed onto the catalysts [3] and signifies a competitive adsorption of hydrogen and the aromatic molecule on a catalyst surface [47]. The strong adsorption of benzene on the catalyst is confirmed via TPSR studies.

Both reversibly and irreversibly adsorbed benzene exists on the catalyst upon reaction and subsequent purging in helium. It was found that as much as 1.11×10^{-4} mol g_{met}^{-1} was desorbed from the catalyst as reversibly adsorbed benzene. In the case of irreversibly adsorbed benzene, hydrogen was required to remove the strongly adsorbed benzene. This leads to the desorption of 1.88×10^{-5} mol g_{met}^{-1} cyclohexane.

Taking these factors into consideration, as well as additional assumptions such as hydrogen adsorbs dissociatively while benzene adsorbs molecularly on similar active sites, we describe the mechanism of reaction as in Eq. (2):

$$r = \frac{kK_E K_{Bz} P_{Bz} K_H^2 P_H^2}{(1 + K_{Bz} P_{Bz})^2} \quad (2)$$

where k is the rate constant, K_H and K_{Bz} as well as P_H and P_{Bz} are the chemisorption constant and partial pressures of the hydrogen and benzene respectively and K_E is the equilibrium constant. The rate determining step (RDS) in this theoretical equation is the addition of the fourth hydrogen atom to an adsorbed benzene molecule. Adsorbed benzene is considered as the main species on the catalyst surface. Plotting $P_H {P_B}^{1/2}/r^{1/2}$ as a function of P_B when P_H is constant results in a fairly good straight line, which gives K_B and $kK_E K_H^2$ values of 44.83 atm^{-1} and 5.01×10^{-3} mol^2 atm^{-2} g_{met}^{-2} min^{-2} respectively. The K_B value which is much larger than unity depicts that benzene is mainly adsorbed on the catalysts. Previous works have reported K_B values between 19 and 5400 atm^{-1} [48,49]. This is dependant on the catalyst as well as the temperature involved. In contrast, the value obtained for the combined $kK_E K_H^2$ does not offer much information. A similar theoretical curve as the experimental was obtained when P_B is constant.

4. Conclusions

In conclusion, it is found that lower activation temperatures are preferable for Pt/Ni bimetallic supported MCM-41 catalysts prepared via classical methods. The higher degree of reduction when the catalyst is activated at high temperatures promotes aggregation that inevitably decreases catalytic reactivity. Studies of the Pt/Ni catalysts of different ratios, activated at low temperatures, demonstrated that the $Pt_{90}Ni_{10}$ and $Pt_{50}Ni_{50}$ catalysts gave rise to improved activity when compared to Pt_{100}. It is believed that this is due to the anchoring effect of Ni^{2+} ions that result in well dispersed Pt particles.

Acknowledgements

The authors would like to acknowledge the financial support from Communauté Urbaine du Grand Nancy, University Sains Malaysia, Université Henri Poincaré, the French and Malaysian governments for the Co-tutelle and ASTS scholarship for N.H.H. Abu Bakar.

References

[1] C.-Y. Lu, H.-H. Tseng, M.-Y. Wey, K.-H. Chuang, J.-H. Kuo, J. Environ. Manage. 90 (2009) 1884.
[2] M.M. Bettahar, R. Wojcieszak, S. Monteverdi, J. Colloid Interf. Sci. 332 (2009) 416.
[3] R. Wojcieszak, S. Monteverdi, M. Mercy, I. Nowak, M. Ziolek, M.M. Bettahar, Appl. Catal. A: Gen. 268 (2004) 241.
[4] A.G. Boudjahem, S. Monteverdi, M. Mercy, M.M. Bettahar, J. Catal. 221 (2004) 325.
[5] R. Wojcieszak, M. Zielinski, S. Monteverdi, M.M. Bettahar, J. Colloid Interf. Sci. 299 (2006) 238.
[6] A. Jasik, R. Wojcieszak, S. Monteverdi, M. Ziolek, M.M. Bettahar, J. Mol. Catal. A: Chem. 242 (2005) 81.
[7] P.-H. Jen, Y.-H. Hsu, S.D. Lin, Catal. Today 123 (2007) 133.

[8] T. Takahashi, S.-I. Higashi, T. Kai, H. Kimura, T. Masumoto, Catal. Lett. 26 (1994) 401.
[9] B. Li, S. Kado, Y. Mukainakano, M. Nurunnabi, T. Miyao, S. Naito, K. Kunimori, K. Tomishige, Appl. Catal. A: Gen. 304 (2006) 62.
[10] Y. Mukainakano, K. Yoshida, S. Kado, K. Okumura, K. Kunimori, K. Tomishige, Chem. Eng. Sci. 63 (2008) 4891.
[11] J.-F. Drillet, A. Ea, J. Friedemann, R. Kotz, B. Schnyder, V.M. Schmidt, Electrochim. Acta 47 (2002) 1983–1988.
[12] M.-K. Min, J. Cho, K. Cho, H. Kim, Electrochim. Acta 45 (2000) 4211.
[13] I. Eswaramoorthi, A.G. Bhavani, N. Lingappan, Appl. Catal. A: Gen. 253 (2003) 469.
[14] X. Han, R. Zhou, B. Yue, X. Zheng, Catal. Lett. 109 (2006) 157.
[15] X.-X. Han, R.-X. Zhou, G.-H. Lai, X.-M. Zheng, Reac. Kinet. Catal. Lett. 83 (2004) 55.
[16] Y. Zhao, E. Yifeng, L. Fan, Y. Qiu, S. Yang, Electrochim. Acta 52 (2007) 5873.
[17] L.J. Simon, P.J. Kooyman, J.G. van Ommen, J.A. Lercher, Appl. Catal. A: Gen. 252 (2003) 283.
[18] S. Lu, W.W. Lonergan, J.P. Bosco, S. Wang, Y. Zhu, Y. Xie, J.G. Chen, J. Catal. 259 (2008) 260.
[19] N.H.H. Abu Bakar, M.M. Bettahar, M. Abu Bakar, S. Monteverdi, J. Ismail, Catal. Lett. 130 (2009) 440.
[20] N.H.H. Abu Bakar, M.M. Bettahar, M. Abu Bakar, S. Monteverdi, J. Ismail, M. Alnot, J. Mol. Catal. A: Chem. 308 (2009) 87.
[21] N.H.H. Abu Bakar, M.M. Bettahar, M. Abu Bakar, S. Monteverdi, J. Ismail, M. Alnot, J. Catal. 265 (2009) 63.
[22] W.W. Lonergan, D.G. Vlachos, J.G. Chen, J. Catal. 271 (2010) 239–250.
[23] A. Lewandowska, S. Monteverdi, M. Bettahar, M. Ziolek, J. Mol. Catal. A: Chem. 188 (2002) 85.
[24] C.H. Bartholomew, R.J. Farrauto, J. Catal. 45 (1976) 41.
[25] D.J. Kang, K.N. Kim, S.G. Kim, J. Mater. Sci. 40 (2005) 6283.
[26] A. Saadi, R. Merabti, Z. Rassoul, M.M. Bettahar, J. Mol. Catal. A: Chem. 253 (2006) 79.
[27] P. Kim, H. Kim, J.B. Joo, W. Kim, I.K. Song, Y. Yi, J. Mol. Catal. A 256 (2006) 178.
[28] J.C. Chaston, Plat. Met. Rev. 8 (1964) 50.
[29] T. Shima, J. Tominaga, Jpn. J. Appl. Phys. 42 (2003) 3479.
[30] J. Rynkowski, D. Rajski, I. Szyszka, J.R. Grzechowiak, Catal. Today 90 (2004) 159.
[31] R. Lanza, P. Canu, S.G. Jaras, Appl. Catal. A: Gen. 348 (2008) 221.
[32] Y. Li, G.-H. Lai, R.-X. Zhou, Appl. Surf. Sci. 253 (2007) 4978.
[33] R.-M. Jao, T.-B. Jao, J.-R. Chang, J. Catal. 161 (1996) 222.
[34] M. Che, Z.X. Cheng, C. Louis, J. Am. Chem. Soc. 117 (1995) 2008.
[35] Y.I. Yermakov, B.N. Kuznetsov, I.A. Ovsyannikov, A.N. Startsev, S.B. Erenburg, M.A. Sheromov, React. Kinet. Catal. Lett. 8 (1978) 377.
[36] S. Lim, C. Wang, Y. Yang, D. Ciuparu, L. Pfefferle, G.L. Haller, Catal. Today 123 (2007) 122.
[37] J.T. Miller, B.L. Meyers, M.K. Barr, F.S. Modica, D.C. Koningsberger, J. Catal. 159 (1996) 41.
[38] A. Punnoose, M.S. Seehra, I. Wender, Fuel Process. Technol. 74 (2001) 33.
[39] S. Mukerjee, S. Srinivasan, M.P. Soriaga, J. McBreen, J. Phys. Chem. 99 (1995) 4577.
[40] H. Yang, C. Coutanceau, J.-M. Léger, N. Alonso-Vante, C. Lamy, J. Electroanal. Chem. 576 (2005) 305.
[41] B. Lim, X. Lu, M. Jiang, P.H.C. Camargo, E.C. Cho, E.P. Lee, Y. Xia, Nano Lett. 8 (2008) 4043.
[42] H. Song, F. Kim, S. Conner, G.A. Somorjai, P. Yang, J. Phys. Chem. B 109 (2005) 188.
[43] S.D. Lin, M.A. Vennice, J. Catal. 143 (1993) 563.
[44] R. Molina, G. Poncelet, J. Catal. 199 (2001) 162.
[45] C. Miradatos, J.A. Dalmon, G.A. Martin, J. Catal. 105 (1987) 405.
[46] P. Marécot, Appl. Catal. 74 (1991) 261.
[47] S. Smeds, T. Salmi, D. Murzin, Appl. Catal. A: Gen. 145 (1996) 253.
[48] H.A. Franco, M.J. Phillips, J. Catal. 63 (1980) 346–354.
[49] K.J. Yoon, M.A. Vannice, J. Catal. 82 (1983) 457–468.